

# Data-Driven Optimization of GPU efficiency for Distributed LLM–Adapter Serving

Ferran Agulló<sup>a,b,1,\*</sup>, Joan Oliveras<sup>a,b</sup>, Chen Wang<sup>c</sup>, Alberto Gutierrez-Torre<sup>a</sup>, Olivier Tardieu<sup>c</sup>, Alaa Youssef<sup>c</sup>, Jordi Torres<sup>a,b</sup>, Josep Ll. Berral<sup>a,b</sup>

<sup>a</sup>Barcelona Supercomputing Center (BSC), Barcelona, Spain

<sup>b</sup>Universitat Politècnica de Catalunya - BarcelonaTech (UPC), Barcelona, Spain

<sup>c</sup>IBM Research, New York, USA

---

## Abstract

Large Language Model (LLM) adapters enable low-cost model specialization, but introduce complex caching and scheduling challenges in distributed serving systems where hundreds of adapters must be hosted concurrently. While prior work has largely focused on latency minimization, resource efficiency through throughput maximization remains underexplored. This paper presents a data-driven pipeline that, for a given workload, computes an adapter placement that serves the workload with the minimum number of GPUs while avoiding request starvation and GPU memory errors. To that end, the approach identifies the maximum feasible throughput attainable on each GPU by leveraging accurate performance predictions learned from real serving behavior. The proposed pipeline integrates three components: (i) a Digital Twin (DT) tailored to LLM-adapter serving, (ii) a distilled machine learning (ML) model trained on DT-generated data, and (iii) a greedy placement algorithm that exploits ML-based performance estimates to maximize GPU efficiency. The DT emulates real system dynamics with high fidelity, achieving below 5% throughput estimation error while executing up to 90× faster than full LLM benchmarking across both predictable and unpredictable workloads. The learned ML models further accelerate performance estimation with marginal accuracy degradation, enabling scalable optimization. Experimental results demonstrate that the pipeline substantially improves GPU efficiency by reducing the number of GPUs required to sustain target workloads. Beyond GPU efficiency, the pipeline can be adapted to alternative objectives, such as latency minimization, highlighting its versatility for future large-scale LLM serving infrastructures.

*Keywords:* Large language models (LLMs), Distributed system, LLM adapters, LoRA adapters, Digital twin, GPU optimization, Machine learning (ML), Performance modeling

---

## 1. Introduction

With the rapid advancement and widespread adoption of Large Language Models (LLMs), the demand for LLM-adapters has grown significantly. While LLMs are large-scale models trained to achieve strong performance across diverse language tasks, adapters specialize this general knowledge to concrete applications through lightweight parameter additions [12, 11, 19, 10]. The use of adapters is far quicker than training-from-scratch or fine-tuning a new model, which is a tedious and long process that requires meticulous data curation and high computation capabilities. Moreover, adapters achieve comparable performance to other equivalent methods such as in-context learning [4] or prompt tuning [18, 24].

As adapters are increasingly used to specialize and deploy LLMs across diverse tasks [32], efficiently managing their inference execution has become a key systems concern [34, 17, 13]. Although adapters were originally designed to be merged into the backbone model to avoid additional computation and preserve latency [12], contemporary serving systems typically keep them unmerged. This design enables the serving of multiple task-specific adapters on top of a shared backbone without replicating its large parameter footprint in GPU memory. Such an approach is particularly well suited for multi-tenant environments, where a system must serve multiple users, each requiring a distinct model specialization [28]. Since adapters are compact, a single GPU can serve hundreds or even thousands of different specializations of the same LLM [29, 5]. This consolidation increases per-GPU throughput by aggregating requests from the hosted adapters whose individual arrival rates are often too low to saturate a GPU.

However, excessive adapter packing can cross a critical threshold where *request starvation* emerges. In this regime, the GPU lacks sufficient memory for intermediate request states (i.e. KV cache), so requests accumu-

---

\*Corresponding author

Email addresses: [ferran.agullo@bsc.es](mailto:ferran.agullo@bsc.es) (Ferran Agulló), [joan.oliveras@bsc.es](mailto:joan.oliveras@bsc.es) (Joan Oliveras), [chen.wang1@ibm.com](mailto:chen.wang1@ibm.com) (Chen Wang), [alberto.gutierrez@bsc.es](mailto:alberto.gutierrez@bsc.es) (Alberto Gutierrez-Torre), [tardieu@ibm.com](mailto:tardieu@ibm.com) (Olivier Tardieu), [asyousse@ibm.com](mailto:asyousse@ibm.com) (Alaa Youssef), [jordi.torres@bsc.es](mailto:jordi.torres@bsc.es) (Jordi Torres), [josep.ll.berral@upc.edu](mailto:josep.ll.berral@upc.edu) (Josep Ll. Berral)

<sup>1</sup>Code will be available at: <https://github.com/FerranAgulloLopez/DistributedEfficientAdapterLLMServing>

late faster than they are processed and latency increases steadily. Determining an allocation that maximizes per-GPU throughput, and thus GPU utilization, without triggering starvation is non-trivial. This optimal point, denoted as  $Max_{pack}$ , depends on the interplay between the sizes and request arrival rates of the adapters, which vary across deployments and over time. Adapter size constrains the GPU memory available for intermediate states and increase computation time, while arrival rate governs the load induced by each adapter.

To mitigate the GPU footprint of adapter weights, serving systems often employ dynamic mechanisms that swap adapters between CPU and GPU memory based on utilization. Adapters resident in GPU memory can execute requests in parallel with other resident adapters [6], while swapping enables interleaved execution among adapters that do not simultaneously coexist on the GPU. Some frameworks, such as vLLM [15], additionally enforce a static upper bound on the number of loaded adapters,  $A_{max}$ , and preallocate the corresponding GPU memory at initialization. This choice directly shapes  $Max_{pack}$ : increasing  $A_{max}$  reduces memory available for request processing, while decreasing it limits achievable parallelism. Improper tuning of  $A_{max}$  can therefore induce starvation and, in extreme cases, GPU memory errors.

Building on these observations, this work addresses the following problem: **given an expected future workload composed of adapters with heterogeneous sizes and request arrival rates, determine a GPU allocation strategy that maximizes per-GPU throughput by achieving  $Max_{pack}$ , so that the workload is served using the minimum number of GPUs without incurring starvation or memory errors.** The solution must also derive the corresponding  $A_{max}$  configuration for each GPU. By *expected future workload*, we focus on *predictable* workloads that can be estimated in advance, such as long-term patterns present in production traces that exhibit periodicity [34]. This formulation enables distributed systems to provision the minimal GPU capacity required for a workload in advance, improving hardware efficiency. We refer to this optimization challenge as the **adapter caching problem**, whose output specifies adapter placement across GPUs together with per-GPU  $A_{max}$  values.

While prior work has explored the optimization of LLM-adapter serving via kernel-level enhancements [6], memory management techniques [29], and scheduling strategies [13], the adapter caching problem remains largely underexplored. The closest related work is dLoRA [34], which, among its contributions, proposes a greedy, heuristic-based algorithm that proactively determines a GPU allocation strategy based on long-term workload patterns. Whereas dLoRA targets latency reduction by exploiting all available resources, our objective is to maximize GPU efficiency by optimizing per-GPU throughput. To this end, we propose a data-driven pipeline comprising three phases: (i) a *Digital Twin* (DT) that emu-

lates an online LLM-adapter serving system; (ii) a machine learning (ML) phase that employs data generated by the DT; and (iii) a greedy algorithm that computes the final adapter placement to solve the caching problem.

Unlike purely heuristic approaches, our method bases allocation decisions on learned system behavior obtained under diverse workload and system conditions. The greedy algorithm exploits this performance knowledge captured by the ML models to approach the optimal packing point,  $Max_{pack}$ , for each GPU, while determining an appropriate  $A_{max}$  configuration. To train the ML models without incurring the prohibitive cost of profiling a real LLM-adapter serving system, we introduce a Digital Twin that reproduces the system’s behavior with orders-of-magnitude faster execution and substantially lower resource consumption. Building this Digital Twin required an in-depth profiling and analysis of the dominant overheads in LLM-adapter serving, which we also report.

We evaluate our approach using the widely adopted vLLM framework [15] with LoRA adapters [12]. To illustrate the generality of the adapter caching problem beyond a single framework, we additionally provide a brief analysis using S-LoRA [29] in Appendix A.

In summary, this work makes the following contributions:

- **A data-driven pipeline to solve the *adapter caching problem*, minimizing the number of GPUs required to serve an anticipated workload** by maximizing per-GPU utilization while avoiding request starvation and memory errors. The pipeline integrates a Digital Twin, an ML learning phase, and a greedy allocation algorithm.
- **To our knowledge, the first Digital Twin that emulates LLM-adapter serving.** It runs orders of magnitude faster than the real system while accurately reproducing key performance metrics and efficiently generating synthetic training data for the ML learning phase.
- **A detailed analysis of the dominant overheads in LLM-adapter serving**, quantifying their interactions under diverse workloads and providing actionable configuration guidelines.

*Paper structure:* The remainder of this work is organized as follows. Sections 2 and 3 present the necessary background and review prior work, with the former also showing the adapter caching problem in practice. Sections 4, 5, 6, and 7 detail the components of the proposed pipeline. Section 8 reports the main experimental results, while Sections 9 and 10 provide discussion and concluding remarks.

## 2. Background

### 2.1. LLM serving

An LLM serving system processes each request through two sequential phases: *prefill* and *decode*. During prefill, all input tokens are processed in parallel, producing intermediate attention states, commonly referred to as the KV cache, which are stored in GPU memory to avoid redundant computation during generation. In the decode phase, output tokens are generated autoregressively, one token at a time, while newly computed KV values are appended to memory. Generation terminates upon emission of an end-of-sequence token or when the maximum output length is reached.

Because decoding is inherently sequential and therefore not compute-intensive, serving systems improve hardware utilization by processing multiple requests in parallel through batching [25]. As static batching is inefficient under variable output lengths, modern systems instead adopt *continuous batching* [37, 15, 22, 21]. It allows requests to dynamically enter and exit the batch between decoding iterations, significantly improving throughput and latency.

At runtime, the number of active requests in the batch is primarily constrained by GPU memory, as each request maintains a growing KV cache throughout decoding. Early frameworks conservatively preallocated memory for the maximum possible output length, resulting in substantial overprovisioning. In contrast, systems such as vLLM [15] and S-LoRA [29] employ greedy KV-cache allocation strategies that reserve memory only for a limited window of upcoming tokens. While this design improves memory efficiency, it may lead to request preemption under high volumes of request arrivals.

### 2.2. (vLLM) Adapter serving

Multiple types of LLM-adapters have been proposed [11, 19, 10, 30]. In this work, we focus on LoRA adapters [12], which remain the most widely adopted approach. LoRA introduces trainable weights into specific layers of the backbone LLM through two low-rank matrices. Their resulting activations are added to the corresponding backbone layer outputs, allowing the adapter to learn only the residual difference between the pretrained and target tasks. The size of a LoRA adapter is defined by the dimensionality of its low-rank latent space, known as *rank*.

Modern serving systems support parallel execution of multiple adapters within the same batch through kernel-level optimizations [6]. Nevertheless, a request can be processed only if both the backbone model and adapter weights reside in GPU memory. Adapter weights therefore reduce the memory available for requests KV cache. To alleviate this limitation, adapters are dynamically swap between CPU and GPU depending on their current usage.

In vLLM, GPU memory is statically partitioned at initialization by reserving a fixed region for adapter weights. This design limits the maximum number of simultaneously loaded adapters, denoted as  $A_{max}$ . Although tunable,

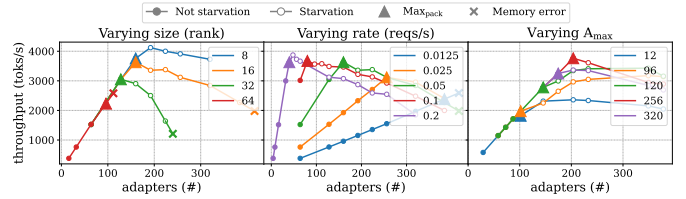


Figure 1: Throughput as a function of the number of served adapters under varying adapter sizes (left), arrival rates (center) and configured  $A_{max}$  (right). Each line corresponds to experiments in which all parameters are held constant except for the number of adapters. Results were obtained using vLLM with Llama-2-7B [31] and a public LoRA adapter [36]. Unless otherwise specified, the default configuration is: adapter size 8 (rank), per-adapter arrival rate 0.05 req/s, 250 input tokens per request, and 231 output tokens per request. In the two leftmost plots,  $A_{max}$  is set equal to the number of served adapters.  $S_{max}$  is configured to match the adapter size used in each experiment.

there is no principled methodology to choose its optimal value. Furthermore, vLLM assigns a uniform maximum memory footprint per adapter,  $S_{max}$ , causing all adapters to occupy identical GPU memory space regardless of their actual size. S-LoRA [29] mitigates these limitations by jointly managing KV-cache and adapter-weight memory within a unified cache. However, given the archival status of its codebase and its limited adoption in practice, it is not used as the primary framework in this study. An exploratory analysis is provided in Appendix A.

### 2.3. Illustrating the adapter caching problem

Fig. 1 illustrates the adapter caching problem under homogeneous workloads on a single GPU. Each curve shows the throughput as a function of the number of concurrently served adapters. Two distinct regimes are consistently observed in each line. Initially, throughput increases approximately linearly as additional adapters introduce more request load that can be efficiently batched together. Beyond a certain point, throughput saturates or degrades due to insufficient GPU memory for KV-cache allocation, resulting in request starvation. The transition between these two regimes marks the optimal packing point  $Max_{pack}$  targeted in this work, which maximizes throughput while avoiding starvation. In practice, we identify this point as the highest measured throughput that remains above 90% of the total incoming token rate.

The location of  $Max_{pack}$  is highly sensitive to adapter size, arrival rate, and the configured value of  $A_{max}$ , as a consequence of the adapter-serving overheads analyzed in Section 5.1. Larger adapters reduce the available memory for request processing and increase computation cost, yielding lower  $Max_{pack}$  points. Lower arrival rates similarly obtain lower peak points, as more adapters are required to saturate GPU memory, increasing adapter overheads. The choice of  $A_{max}$  introduces a trade-off between reserving excessive memory for adapters (e.g.,  $A_{max} = 320$ ) and restricting achievable parallelism (e.g.,

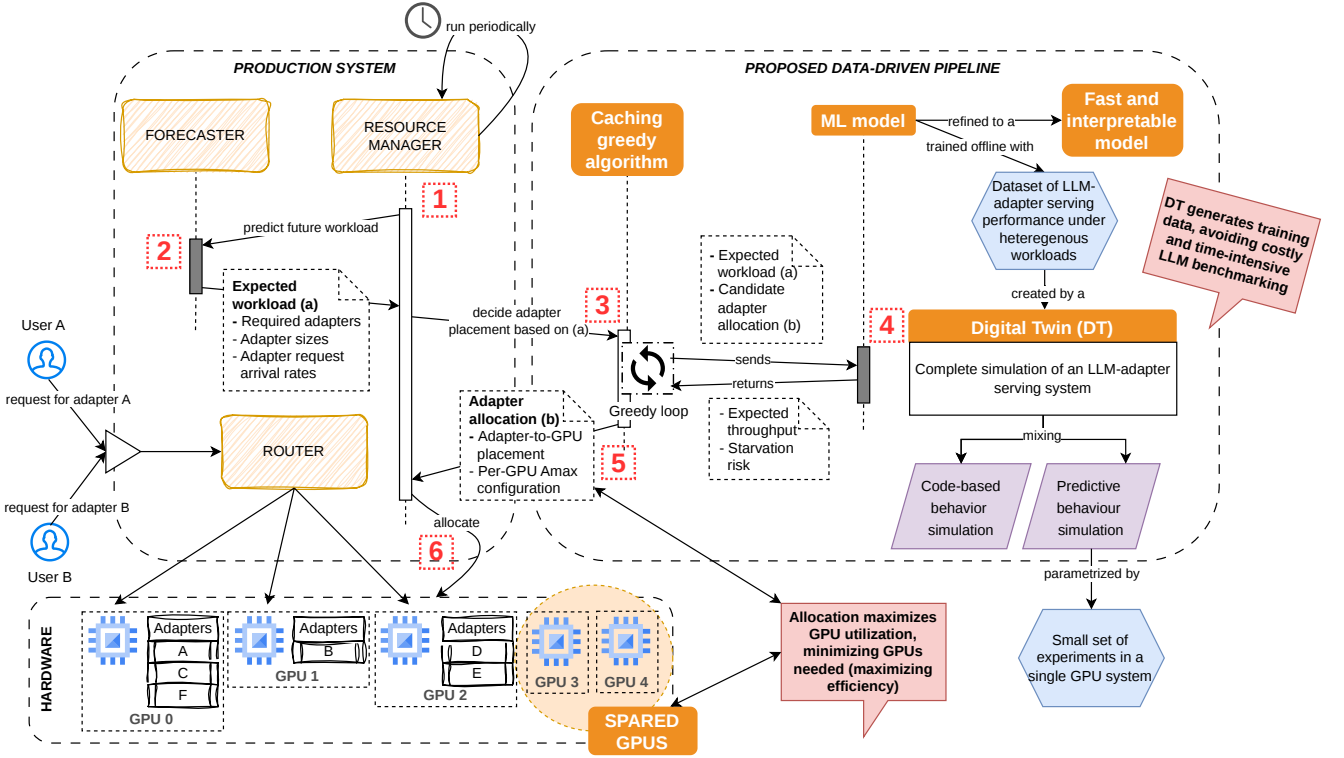


Figure 2: Proposed data-driven pipeline to address the adapter caching problem (right), shown alongside its expected usage within a production system (left). The numbered red markers indicate the recommended reading order of the workflow.

$A_{max} = 96$ ). While the results shown correspond to homogeneous workloads, substantially higher variance arises under heterogeneous adapter sizes and arrival rates. Lastly, memory errors (marked as crosses) occur for large adapter sizes and low arrival rates as  $A_{max}$  is trivially set equal to the number of served adapters, resulting in the reservation of more GPU memory for adapter weights than is available.

### 3. Related work

#### 3.1. LLM adapter optimization

A growing body of work has focused on improving the efficiency of LLM-adapter serving systems. Existing approaches can be broadly categorized into three levels: kernel-level optimizations, such as Punica [6], which enables batching requests across multiple adapters; memory-level optimizations, exemplified by S-LoRA [29], which extends vLLM by dynamically partitioning GPU memory across both requests and adapters; and scheduler-level techniques, including CaraServe [17], Chameleon [13], and dLoRA [34].

CaraServe reduces cold-start overheads and optimizes request scheduling for heterogeneous adapter sizes, while Chameleon improves adapter cache management and introduces an express-lane mechanism for short requests. Both systems present detailed performance analyses, with

CaraServe focusing mainly on the computational overhead of mixing adapters and Chameleon emphasizing Time To First Token (TTFT) and adapter loading time.

The work most closely related to ours is dLoRA [34], which proposes a distributed adapter-serving system that incorporates placement decisions based on both short-term and long-term workload patterns observed in production traces. For short-term dynamics—largely driven by unpredictable output lengths—dLoRA employs a reactive Integer Linear Programming (ILP)-based optimization to update placement decisions at runtime. For longer-term and more predictable workload patterns, it adopts a heuristic-based algorithm that operates in a proactive manner. Both strategies aim to minimize request latency while utilizing all available resources.

In contrast, our work focuses on long-term behavior and targets GPU resource efficiency, a largely unexplored dimension in prior studies. We adopt a data-driven approach grounded in real system behavior and complement it with a detailed performance analysis of adapter-serving overheads. In particular, we emphasize throughput and Inter-Token Latency (ITL), which form the foundation for the development of our proposed Digital Twin.

#### 3.2. LLM simulators or digital twins

Several simulators have been proposed to model default LLM serving behavior. Vidur [1] aims to simplify server configuration selection by training random forest

models on benchmarking data to predict performance metrics. LLMervingSim [7] emulates the continuous batching loop of LLM serving systems and is primarily intended for architecture exploration. Beyond simulators, more specific analytical performance models have also been proposed. Latency is commonly approximated as a linear function of batch size, following earlier studies on generic AI models [38, 27]. In the context of adapter serving, CaraServe [17] models adapter computation latency as a linear function of batch size and either the sum or the maximum adapter size within the current batch.

To the best of our knowledge, no existing simulator or digital twin explicitly models the combined dynamics of adapter caching, KV-cache allocation, and continuous batching in multi-adapter LLM serving. Our Digital Twin combines code-based simulation with predictive behavior modeling. The latter relies on performance models that reuse existing analytical formulations where applicable, while incorporating additional components and refinements to accurately capture adapter-serving behavior under heterogeneous workloads.

### 3.3. Extension of prior workshop version

A preliminary version of this work was presented at the NeurIPS ML for Systems Workshop (2025) [20], where throughput maximization was addressed in single-GPU settings via  $Max_{pack}$  estimation. This manuscript substantially extends that work by generalizing the problem to distributed multi-GPU environments and introducing a greedy placement algorithm for adapter allocation. Moreover, the ML component is reformulated as a distilled surrogate of the Digital Twin (DT), enabling efficient performance prediction to guide placement under heterogeneous workloads. Finally, the experimental evaluation is significantly expanded, including validation under unpredictable arrival patterns and distributed scenarios not considered in the workshop version.

## 4. Pipeline overview

Fig. 2 illustrates the proposed data-driven pipeline and its expected integration within a production system. Inspired by the long-term predictive strategy of dLoRA, the pipeline is designed to be periodically reinvoked based on an anticipated workload. A workload is characterized by the required adapters, their sizes, and their request arrival rates. Given this workload, the pipeline computes an adapter-to-GPU placement together with the optimal  $A_{max}$  configuration per device. The resulting allocation maximizes per-GPU utilization by driving a subset of devices to their maximum feasible packing throughput ( $Max_{pack}$ ), thereby minimizing the number of GPUs required to serve the workload. The remaining devices can be reassigned to other workloads to improve overall system efficiency or powered down to reduce energy consumption.

The pipeline consists of three components: (i) a Digital Twin (DT), (ii) an ML learning phase, and (iii) a

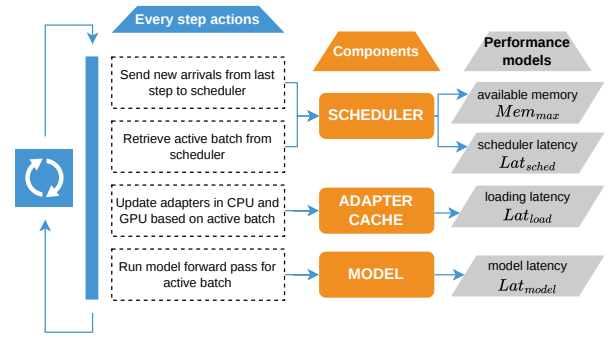


Figure 3: Digital Twin behavior and architecture.

greedy adapter caching algorithm. The greedy algorithm produces the final placement decision, relying on performance predictions generated by the ML models. Trained offline, these models estimate the achievable throughput of a GPU under a given adapter placement and  $A_{max}$  configuration, and predict whether starvation may arise. An optional refinement phase can simplify the models into faster and more interpretable surrogates, at the cost of limited accuracy degradation.

Training such models requires a large and diverse dataset capturing LLM-adapter serving behavior across heterogeneous workloads. Exhaustively constructing this dataset via real-system benchmarking is computationally prohibitive due to its execution time and resource cost. To overcome this limitation, we introduce a Digital Twin that emulates the internal dynamics of an LLM-adapter serving system through a combination of code-based and predictive behavior simulation. The DT operates orders of magnitude faster and with substantially lower resource consumption than full-system benchmarking, enabling large-scale synthetic data generation to train the ML models. While the DT provides high-fidelity performance estimates, it is not directly invoked by the greedy caching algorithm, as the ML surrogate enables significantly faster inference and improved interpretability, making the pipeline suitable for production deployment. Prior to use, the DT requires a lightweight parameterization phase based on a small set of benchmarking experiments executed on the target hardware and model configuration.

## 5. Digital twin

The proposed Digital Twin (DT) reproduces the behavior of an online LLM-adapter serving system. Rather than acting as a simple performance metric estimator, the DT emulates system state transitions and execution dynamics within the continuous batching loop that characterizes modern serving frameworks. This design enables accurate performance estimation under heterogeneous and diverse workload distributions. The DT operates offline and exclusively on CPU to facilitate cost-efficient generation of training data for the ML models. Offline execution refers

to advancing a simulated clock while accounting for real execution time, thereby avoiding idle waiting and preserving the possibility of easily extending the approach to an online simulation if required.

The DT is built on a set of modular components, each modeling a specific part of the real system. These components reproduce system behavior through simplified yet structurally analogous logic (code-based simulation) and integrate lightweight predictive performance models to estimate the latency of the most computationally intensive operations without executing them.

As depicted in Fig. 3, each simulation step begins by injecting new request arrivals according to the real execution time and the workload arrival distribution. Requests are then passed to the scheduler, which updates the active batch by removing completed requests and admitting new ones. Following the design of vLLM, a greedy KV-cache allocation strategy is applied. The updated batch is subsequently processed by the adapter cache and model components, which emulate adapter loading/unloading as well as the model forward pass, respectively.

As a standard Digital Twin, the DT requires the same inputs as the real system to perform the simulation. These include the execution duration and detailed workload characteristics, namely the arrival time of each request, the target adapter, adapter size, request input length, and the configured GPU  $A_{max}$  value. Unlike the real system, however, the DT does not internally derive the amount of output tokens per request. Instead, the expected output length must also be provided as an input parameter. Nevertheless, our evaluation shows that using the average output length across requests yields sufficiently accurate performance estimates while remaining practical to approximate in production environments. By reproducing all major execution stages of a real serving system, the DT can generate a wide range of performance metrics, including throughput, ITL, and TTFT.

### 5.1. Performance analysis

We describe the four main overheads that we encountered when working with adapters. This exploration represents the foundation for the design and implementation of the DT and its predictive performance models. Experiments setup is described in Section 8.1.

#### 5.1.1. Increased memory usage

As introduced, storing adapter weights in GPU memory reduces the capacity available for the requests KV-cache, which limits the batch size and thus the throughput. Fig. 4 shows this decrease in both batch size and throughput, which appears earlier and more sharply for larger models and adapters due to their higher memory footprint. Unexpectedly, throughput decays exponentially rather than linearly as batch size. This discrepancy arises from a broader trait of LLM serving unrelated to adapter processing. As reported in several works, increasing the batch

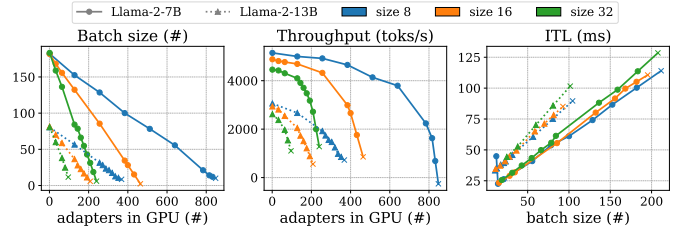


Figure 4: Evolution of batch size and throughput with increasing numbers of loaded adapters (left, center) and ITL versus batch size (right), across models and adapter sizes. Crosses denote the point where GPU memory is exhausted. Measurements were obtained by oversaturating a single-GPU system and issuing backbone-only requests to isolate the memory overhead of adapter weights. Minor variations in ITL across adapter sizes are nevertheless observed, likely due to additional operations triggered in vLLM when adapters are activated, even if unused.

size beyond a certain point leads to diminishing returns in throughput—a phenomenon known as the throughput plateau [25, 26, 2]. This implies that, for example, with Llama-2-7B although the first 100 loaded adapters reduce the batch size, their impact on throughput is negligible, a characteristic that, to the best of our knowledge, we are the first to report. Lastly, the rightmost plot of Fig. 4 presents the relationship between ITL and batch size, which, consistent with prior reports for generic AI models [38, 27], exhibits a linear scaling trend.

**Insight.** Each loaded adapter affects throughput, depending on model and adapter size—but this impact may fade due to the throughput plateau.

#### 5.1.2. Increased computational workload

Fig. 5 shows the throughput slowdown and ITL overhead caused by the additional computation and GPU internal transfers required to process adapters instead of only the backbone LLM. Both metrics increase approximately linearly with the number of adapters, except for the sharp drop from zero to one adapter. This drop corresponds to the shift from a backbone-only setup to one that must compute both backbone and adapter activations, including the additional GPU data transfers involved. Beyond this point, computation and transfer overheads from multiple adapters is partially parallelized. Adapter size has a limited impact, with size 32 occasionally yielding lower overhead than size 16.

**Insight.** Serving adapters introduces computational overhead in both throughput and ITL compared to backbone-only execution, increasing linearly with the number of adapters.

#### 5.1.3. Loading time

Fig. 6 presents the loading time to GPU memory relative to request latency, distinguishing between loading from disk and from CPU memory. Larger adapters introduce greater overhead due to their increased size, and disk loading is on average 70% slower than CPU loading. Request length also strongly affects the relative impact:

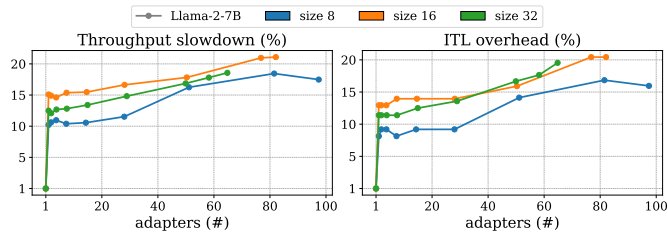


Figure 5: Throughput slowdown and ITL overhead for increasing adapters across three adapter sizes. Results are shown for Llama-2-7B and relative to backbone-only execution. To avoid the impact of adapter weights, we fix the batch size and number of loaded adapters within each line. Lines are shorter for larger adapter sizes due to their reduced achievable batch size, which limits the maximum number of runnable adapters.

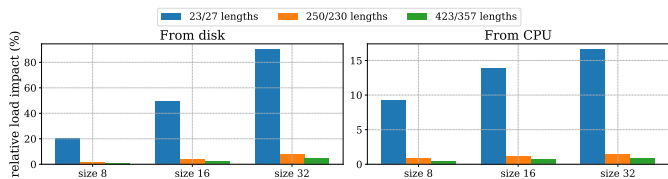


Figure 6: Loading times for varying adapter sizes, shown relative to request latency across three input/output lengths for Llama-2-7B and storage type. Request latency is computed as  $T_{POT} * (output\_tokens - 1)$ , where TPOT is the time per output token.

for small requests, CPU loading adds 7–16% latency depending on adapter size, whereas for longer requests the overhead falls below 2%. This reduction occurs because the fixed cost of loading becomes negligible compared to the computation time of longer requests.

**Insight.** Loading overhead is significant only for short requests and can be largely mitigated by preloading adapters into CPU memory.

#### 5.1.4. Scheduler

Fig. 7 shows the relative impact of the scheduler component across varying numbers of adapters and configured  $A_{max}$ . When the number of adapters is high but  $A_{max}$  is small, scheduling accounts for nearly 6% of execution time; in all other cases, its impact is negligible. This behavior is specific to the vLLM implementation rather than to LLM adapter serving in general. It occurs because vLLM iterates over all pending requests to select those admissible to the active batch; with small  $A_{max}$ , the scheduler must scan a larger fraction of requests to find those corresponding to loaded adapters, as requests from unloaded adapters cannot be processed because  $A_{max}$  has already been reached.

**Insight.** The scheduler component of vLLM may introduce an overhead when  $A_{max}$  is small relative to the number of adapters.

## 5.2. Predictive performance models

As illustrated on the right side of Fig. 3, the Digital Twin relies on four predictive performance models, summarized in Equation (1). Three of these models estimate task-specific latency— $Lat_{sched}$ ,  $Lat_{load}$  and  $Lat_{model}$ —while

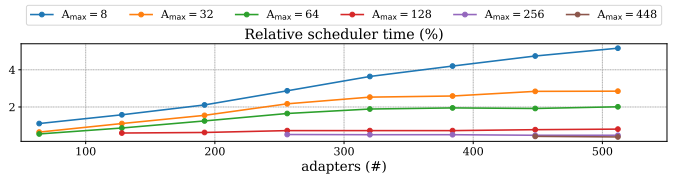


Figure 7: Scheduler time relative to the average per-step execution time, as a function of the number of adapters and configured  $A_{max}$ .

the fourth,  $Mem_{max}$ , serves as an auxiliary estimator used by the scheduler to determine the maximum number of requests that can be batched together under the memory pressure introduced by adapter weights (see Section 5.1.1). Specifically,  $Mem_{max}$  takes  $A_{max}$  and  $S_{max}$  as inputs and outputs the maximum number of request tokens that can fit within GPU memory ( $T_{max}$ ). This estimator is derived directly from profiled data, analogous to the leftmost plot in Fig. 4, but estimates the achievable token count rather than batch size. Although an analytical formulation could be derived from backbone and adapter sizes, using empirical profiling results proved more straightforward and equally accurate.

The latency model  $Lat_{sched}$  is used by the scheduler to estimate the time spent in the original vLLM scheduling component. It takes as input the batch size ( $B$ ), the number of pending requests ( $R_P$ ), the number of unique adapters currently in the batch ( $A_B$ ), and the total number of adapters being served ( $A$ ). Its formulation follows a parameterized analytical expression with constants calibrated through profiling. The first two terms represent the baseline scheduling behavior: an iteration over the active batch to detect completed requests and manage KV allocation, followed by a partial iteration over pending requests to assess their eligibility for inclusion. The final term models the overhead described in Section 5.1.4, which accounts for the additional execution time caused by scheduler-specific inefficiencies.

The model  $Lat_{load}$  estimates the time required to load adapters during swapping ( $L$ ) as a function of their size  $S$  (see Section 5.1.3), assuming unloading is negligible. Similar to  $Mem_{max}$ , this model is derived directly from profiled data, specifically the measurements used to generate Fig. 6. Loading is modeled from CPU memory, since disk loading is treated as a one-time initialization cost.

Finally,  $Lat_{model}$  estimates the latency arising from GPU transfers and model forward pass. It is decomposed into two components: the backbone LLM latency ( $Lat_{backbone}$ ) and the additional computational overhead from serving adapters ( $Overhead_A$ ). The backbone latency is modeled as a linear function of batch size, consistent with prior work [38, 27] and supported by the profiling results in the rightmost plot of Fig. 4. The adapter-related overhead is modeled as a linear function of the number of adapters, following the findings in Fig. 5, which differs from previous modeling [17]. The constants for both components are parametrized from the profiling data shown in

the referenced figures.

$$\begin{aligned}
Mem_{max}(A_{max}, S_{max}) &= T_{max} \\
Lat_{sched}(B, R_P, A_B, A) &= K_1 B + K_2 R_P + K_3 R_P \frac{A_B}{A} \\
Lat_{load}(S_A) &= L_A \\
Lat_{model}(B, A) &= Lat_{backbone} * Overhead_A \\
&= (K_4 B + K_5) * (K_6 A + K_7)
\end{aligned} \tag{1}$$

where all constants  $K_x$  are parametrized with benchmarking data on the chosen backbone LLM, adapter types, and hardware configuration.

## 6. ML modeling

The ML phase produces two predictive models that estimate, for a single-GPU setting, (i) achievable throughput and (ii) starvation risk for a given workload, adapter placement and  $A_{max}$  configuration. These estimators are repeatedly invoked by the greedy caching algorithm to guide distributed placement decisions. We adopt classical machine learning techniques, including Random Forests and Support Vector Machines, which provide strong predictive accuracy with moderate computational overhead. An optional refinement phase further reduces inference latency and improves interpretability, both critical for scalable and accountable production deployment.

The models are trained on a performance dataset generated by executing the Digital Twin across a wide range of workload and device configurations. Each simulated scenario contributes one sample consisting of: (i) a feature vector encoding workload and device characteristics, (ii) the DT-estimated throughput, and (iii) a binary starvation indicator. Starvation is defined as the condition where DT-estimated throughput falls below 90% of the total incoming token rate. Although the DT supports arbitrary workload distributions, training data is restricted to long-term workload patterns that can be anticipated in advance. In practice, request arrivals are modeled as a Poisson process with different arrival rates, and simulations use the average input and output token lengths of requests, which are assumed to be predictable in production environments.

The feature vector characterizes both the expected workload and the GPU configuration, comprising: the number of served adapters  $A$ ; the sum and standard deviation of adapter arrival rates; the maximum, mean, and standard deviation of adapter sizes; and the configured  $A_{max}$  value. Two independent models are trained: a regression model for throughput prediction and a binary classifier for starvation detection.

### 6.1. Refinement phase

Among all evaluated model families, tree-based models achieve the best trade-off between predictive accuracy and

interpretability. We therefore further refine these models along two complementary dimensions: inference efficiency and interpretability. Starting from the best-performing trained model, we progressively reduce model complexity until obtaining a single shallow decision tree. To this end, the hyperparameter optimization process is modified to strongly penalize complex structures. Model complexity is quantified as the number of logical decision rules of the form "condition<sub>1</sub>  $\wedge$  condition<sub>2</sub>  $\wedge$   $\dots$   $\rightarrow$  output" into which a decision tree can be decomposed. After complexity reduction, inference performance is further optimized by extracting the learned decision logic and re-implementing it in plain Python, accelerated using Numba [16]. This approach removes framework overhead and leverages code compilation to generate efficient machine code. Overall, this refinement phase substantially reduces inference latency and improves model interpretability, at the cost of a moderate degradation in predictive accuracy.

## 7. Caching greedy algorithm

The greedy caching algorithm constitutes the final stage of the proposed pipeline. Its objective is to solve the adapter caching problem by minimizing the number of GPUs required to serve a given workload through appropriate adapter placement and  $A_{max}$  configuration, while avoiding starvation and memory errors. The algorithm leverages the ML models to estimate the expected throughput and starvation risk associated with candidate GPU allocations and device configurations.

This problem can be viewed as a sophisticated variant of the bin packing problem [8], and is therefore NP-hard. To address it efficiently, we adopt a tailored variation of the First-Fit Decreasing (FFD) algorithm [14], adapted to the specific constraints and objectives of the adapter caching problem.

The pseudocode is shown in Algorithm 1. The algorithm takes as input the expected future workload, defined by the set of adapters to serve ( $A$ ), and for each adapter  $a \in A$ , its expected size  $s[a]$  and arrival rate  $\lambda[a]$ . It also receives the total number of GPUs in the system ( $G$ ). The outputs are the GPU assignment of each adapter ( $g[a]$ ) and the configuration of  $A_{max}$  per GPU ( $A_{max}[g]$ ). If no starvation-free allocation is feasible, the algorithm raises an exception to enforce the non-starvation constraint.

The algorithm follows a greedy strategy, allocating adapters sequentially to maximize GPU packing up to the optimal point  $Max_{pack}$ . Allocation order is determined by the PRIORITYSORTING step: adapters are first sorted by size (largest first) and then by arrival rate in a zigzag order (alternating between high and low) while preserving size-based ordering. Sorting by size groups adapters with similar sizes and prioritizes larger ones first, thereby preventing newly allocated adapters from increasing  $S_{max}$  device configuration. The zigzag ordering was selected empirically, as it consistently improved throughput in our

experiments. Exhaustive per-adapter testing is infeasible, so the algorithm performs provisional allocations via `PROVISIONALINCLUDE` until a predefined testing point is reached (`REACHTESTINGPOINT`). At that point, feasibility is evaluated: successful allocations are committed (`COMMITALLOCATION`), while failed ones are rolled back (`ROLLBACKALLOCATION`), merged back into the pending queue (`MERGE`), and retried on another GPU. In this work, testing points correspond to cumulative adapter counts [8, 16, 32, 64, 96, 128, 160, 192, 256, 320, 384]. After the main loop terminates, any remaining provisional allocations are validated and committed.

---

**Algorithm 1** Caching greedy algorithm

---

**Input:** GPUs  $G = \{g_1, \dots, g_M\}$ ; adapters  $A = \{a_1, \dots, a_N\}$ ; sizes  $s[a]$ ; rates  $\lambda[a]$

**Output:** Assignment  $g[a]$ ; configuration  $A_{max}[g]$

- 1:  $g[a] \leftarrow \emptyset$  **for all**  $a \in A$ ;  $A_{max}[g] \leftarrow 0$  **for all**  $g \in G$
- 2:  $A \leftarrow \text{PRIORITYSORTING}(A, \text{key} = (\lambda[a], s[a]))$
- 3:  $A_q \leftarrow \text{QUEUE}(A)$ ;  $G_q \leftarrow \text{QUEUE}(G)$
- 4: **while**  $A_q \neq \emptyset$  **do**
- 5:    $a \leftarrow \text{POPLEFT}(A_q)$
- 6:   **if**  $G_q = \emptyset$  **then** ERROR STARVATION
- 7:    $g \leftarrow \text{POPLEFT}(G_q)$
- 8:   `PROVISIONALINCLUDE`( $g, a, s[a], \lambda[a]$ )
- 9:   **if** `REACHTESTINGPOINT`( $g$ ) **then**
- 10:      $(ok, alloc\_set, p_{new}) \leftarrow \text{TESTALLOCATION}(g)$
- 11:     **if**  $ok$  **then**
- 12:       `COMMITALLOCATION`( $g$ )
- 13:       **for all**  $a' \in alloc\_set$  **do**  $g[a'] \leftarrow g$
- 14:        $A_{max}[g] \leftarrow p_{new}$
- 15:       `PUSHLLEFT`( $G_q, g$ )
- 16:     **else**
- 17:        $un\_alloc\_set \leftarrow$
- 18:       `ROLLBACKALLOCATION`( $g$ )
- 19:        $A_q \leftarrow \text{MERGE}(A_q, un\_alloc\_set)$
- 20:     **end if**
- 21:     **else**
- 22:       `PUSHLLEFT`( $G_q, g$ )
- 23:     **end if**
- 24: **end while**
- 25: **for all**  $g \in G$  **with** non-tested allocation **do**
- 26:    $(ok, alloc\_set, p_{new}) \leftarrow \text{TESTALLOCATION}(g)$
- 27:   **if** not  $ok$  **then** ERROR STARVATION
- 28:   repeat lines 12-14
- 29: **end for**
- 30: **return** (Assignment  $g[a]$ , configuration  $A_{max}[g]$ )

---

Feasibility is evaluated by the `TESTALLOCATION` method, which also determines the optimal  $A_{max}$  configuration. Its pseudocode is shown in Algorithm 2. The method receives as input the GPU under evaluation and its internal state, including the number of firmly allocated adapters, the set of provisionally included adapters, and their respective sizes and arrival rates. For brevity, internal state management is omitted from the pseudocodes.

The method first queries the ML model for throughput predictions using `MLPREDICTTHROUGHPUT`, evaluating the GPU state under two configurations: the current  $A_{max}$  and the next candidate. As with adapter allocation, exhaustive exploration of all configurations is intractable. Instead, candidate  $A_{max}$  values are restricted to a predefined set returned by `NEXTGPUCONFIG`, which reuses the same array of adapter counts defined earlier. The configuration yielding the highest predicted throughput is selected. Subsequently, the method invokes `MLPREDICTSTARVATION` to check whether the selected configuration, given the current GPU internal state, would lead to starvation. If starvation is predicted, the allocation is rejected as infeasible; otherwise, the method returns the set of new allocatable adapters along with the chosen  $A_{max}$  configuration.

---

**Algorithm 2** `TESTALLOCATION`( $g$ )

---

**Input:** GPU  $g$ ; internal state =  $(\mathcal{A}_{alloc}, \mathcal{A}_{prov}, s[\cdot], \lambda[\cdot], p)$

**Output:** ( $ok, alloc\_set, p_{new}$ )

- 1:  $p_{next} \leftarrow \text{NEXTGPUCONFIG}(g)$
- 2:  $\mathcal{A}_{all} \leftarrow \mathcal{A}_{alloc} \cup \mathcal{A}_{prov}$
- 3:  $T \leftarrow \text{MLPREDICTTHROUGHPUT}(\mathcal{A}_{all}, s[\cdot], \lambda[\cdot], p)$
- 4:  $T_{next} \leftarrow \text{MLPREDICTTHROUGHPUT}(\mathcal{A}_{all}, s[\cdot], \lambda[\cdot], p_{next})$
- 5: **if**  $T > T_{next}$  **then**  $p_{best} \leftarrow p$  **else**  $p_{best} \leftarrow p_{next}$
- 6:  $starve \leftarrow \text{MLPREDICTSTARVATION}(\mathcal{A}_{all}, s[\cdot], \lambda[\cdot], p_{best})$
- 7: **if**  $starve$  **then return** (FALSE,  $\emptyset, \emptyset$ )
- 8: **return** (TRUE,  $\mathcal{A}_{prov}, p_{best}$ )

---

## 8. Evaluation

This section evaluates the Digital Twin and ML learning phase in approximating real LLM-adapter serving behavior, and the effectiveness of the caching greedy algorithm in addressing the adapter caching problem.

### 8.1. Setup

Follows detailed information about the experimental setup:

**Data.** We sample requests from a cleaned version of the ShareGPT dataset [3], preserving their original heterogeneous input and output lengths. Nevertheless, for the data used to parametrize the DT performance models, we generate synthetic requests composed of random words from the `/usr/share/dict/words` file of Unix systems to avoid bias in request content.

**Metrics.** In all textual references, figures, and tables, *throughput* denotes the total processing rate, computed as the sum of input throughput (tokens processed as input) and output throughput (tokens generated as output).

**LLM models.** We use Llama-3.1-8B-Instruct [9] and Qwen2.5-7B-Instruct [35] with LoRA adapters of different sizes derived from two HuggingFace adapters [33, 39]. As of Section 5.1, developed early in this work, we test Llama-2-7B and Llama-2-13B models [31] with LoRA adapters

also based on a HuggingFace adapter [36]. In all experiments, we set  $S_{max}$  as the maximum adapter size found in every tested scenario, which is the default behaviour expected in vLLM.

**ML learning phase.** We evaluate three model types: K-Nearest Neighbors (KNN), Random Forest (RF), and Support Vector Machine (SVM), all coming from the Python scikit-learn library [23]. Training is performed with 5-fold cross-validation, and hyperparameter tuning is conducted using the HalvingGridSearchCV method from scikit-learn. The details of the hyperparameter search space are reported in Appendix B.

**Framework.** All experiments are conducted with vLLM version *v0.8.5*, except for the analyses in Section 5.1, which was performed earlier using version *v0.5.0.post1*. In terms of implementation, we introduce minor modifications to the server components to collect auxiliary metrics and support additional arguments, and substantially update the benchmarking script to better emulate realistic online environments with adapters. When using multiple GPUs, a separate vLLM instance runs on each GPU, and requests are routed according to the output of the greedy algorithm.

**Hardware.** All experiments are conducted on a node equipped with four NVIDIA Hopper H100 (64GB HBM2), 512GB RAM memory, and 80 CPU cores. When running the Digital Twin, the GPU is not utilized.

## 8.2. Digital Twin

We evaluate the accuracy of the proposed Digital Twin (DT) by comparing its predicted performance metrics against those measured on a real LLM-adapter serving system, assessing its ability to reproduce system behavior across a wide range of different workloads. These are generated through a Cartesian combination of two adapter-size sets—high-to-low  $\{8, 16, 32\}$  and medium-to-low  $\{8, 16\}$ —and two arrival-rate regimes—high  $\{1.6, 0.8, 0.4\}$  and low  $\{0.1, 0.05, 0.025\}$  requests per second. For each workload, adapters randomly select a size and a Poisson arrival rate from the chosen sets, producing heterogeneous configurations. The number of served adapters is varied from 8 to 384, and the corresponding values of  $A_{max}$  are explored within the same range. Real-system experiments are executed for one hour per configuration. DT accuracy is quantified using the Symmetric Mean Absolute Percentage Error (SMAPE) across all scenarios. Results are summarized in Table 1 under the *Predictable arrivals* setting. Two variants of DT input information regarding request lengths are evaluated. In the *Original* variant, the DT receives the exact input and output token lengths observed in the real system. In the *Mean* variant, all requests use identical token lengths equal to the workload average. This latter configuration reflects the information typically available in practice and corresponds to the setup used during the ML learning phase.

Overall, the DT accurately reproduces real-system behavior under predictable workloads for both models.

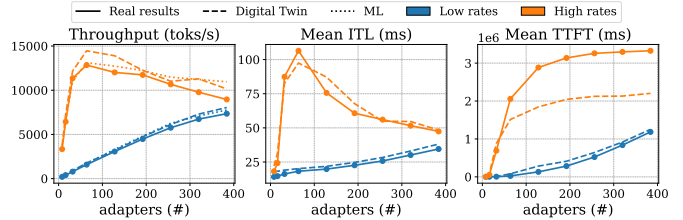


Figure 8: Comparison between Digital Twin predictions and real-system measurements for throughput, ITL, and TTFT under varying numbers of adapters and arrival rates. Experiments are conducted using adapter sizes 8 and 16 on the Qwen-2.5-7B model with  $A_{max} = 8$ , in the predictable setting and *Mean* version. For throughput, predictions produced by the ML model are also reported.

Throughput and ITL achieve maximum SMAPE values of 5.08% and 9.63%, respectively, while TTFT exhibits higher deviation, with a maximum SMAPE of 18.95%. Although the *Original* variant consistently yields lower error, the *Mean* configuration remains comparably accurate, supporting its use in practical scenarios.

Table 2 shows DT time and resource consumption. It achieves up to a  $90\times$  speedup compared to one-hour real-system executions, while requiring minimal resources: a single CPU core, no GPU, and approximately 200 MB of memory. Fig. 8 illustrates a comparison between DT predictions and real-system measurements for a subset of the tested scenarios. Consistent with the aggregated results, throughput and ITL are closely matched, whereas TTFT shows larger deviations, particularly under higher arrival rates.

**Unpredictable arrivals:** We further evaluate the robustness of the Digital Twin under unpredictable arrivals. To that end, each adapter independently updates its arrival process every five minutes. At each update, the arrival distribution is randomly selected between Poisson and log-normal, and the corresponding arrival rate is randomly multiplied or divided by a factor of two. To prevent unrealistic behaviors, arrival rates are clipped within predefined bounds. This configuration generates strongly non-stationary traffic patterns, providing a challenging setting for assessing the DT’s ability to reproduce system behavior under rapidly changing workloads. An example of the resulting arrival traces is shown in the left plot of Fig. 9.

We follow the same evaluation methodology as in the predictable-arrival experiments; however, for efficiency reasons, the number of evaluated scenarios is reduced. Adapter sizes are fixed to 8,  $A_{max}$  is set to 32, and the number of served adapters is varied among 32, 64, and 128. Arrival rates follow the same ranges as in the previous experiments. The resulting SMAPE values are reported in the right part of Table 1.

Overall, the DT accurately reproduces system behavior under unpredictable arrival patterns, achieving error levels comparable to those observed for predictable workloads, albeit slightly lower due to the reduced evaluation

Model	Req. lengths	Predictable arrivals			Unpredictable arrivals		
		SMAPE comparison (%)			SMAPE comparison (%)		
		Through.	ITL	TTFT	Through.	ITL	TTFT
Llama	Original	<b>2.25</b>	<b>7.09</b>	18.83	<b>1.00</b>	<b>3.55</b>	<b>13.92</b>
	Mean	4.18	9.63	<b>17.44</b>	2.06	9.87	21.28
Qwen	Original	<b>2.59</b>	<b>7.18</b>	18.95	<b>1.71</b>	<b>3.54</b>	<b>12.26</b>
	Mean	5.08	9.07	<b>17.92</b>	4.29	5.60	21.49

Table 1: Final evaluation of the proposed Digital Twin across all predictable (left) and unpredictable (right) test scenarios. Reported values correspond to SMAPE between Digital Twin predictions and real-system measurements, where lower values denote higher fidelity.

Model	Resource consumption		
	Time (s)	CPU (%)	Mem (MB)
Llama	38.94 ± 5.58	89.51 ± 1.69	202.58 ± 10.85
Qwen	39.61 ± 5.55	90.33 ± 1.30	204.32 ± 9.29

Table 2: Execution time and resource consumption results of the Digital Twin across all tested scenarios.

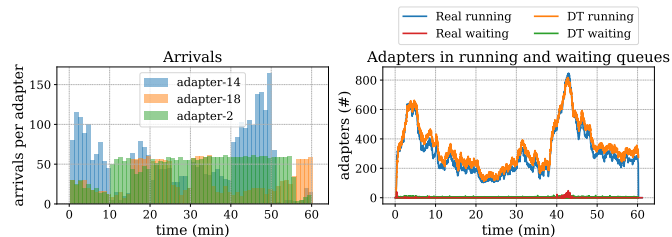


Figure 9: Execution with Llama-3.1-8B under initial high arrival rates (1.6, 0.8, 0.4) for 32 adapters in the unpredictable regime. (Left) Non-stationary arrival traces for randomly sampled adapters. (Right) Comparison of running and waiting requests over time between the Digital Twin and the real system.

space. The right plot of Fig. 9 illustrates the evolution of running and waiting requests over time for both the DT and the real system in a specific scenario. The close alignment between the two traces highlights the DT’s ability to replicate scheduler dynamics, greedy KV-cache allocation, adapter loading behavior, and computation latency under highly dynamic traffic conditions.

### 8.3. ML modeling

Leveraging the Digital Twin for rapid data generation, we train the proposed ML models over an extended and diverse set of workload scenarios. Workloads are generated through a Cartesian product of adapter sizes and arrival rates. Instead of evaluating only a small number of predefined sets, we construct all combinations of three values drawn from the adapter-size set  $\{8, 16, 32\}$  and the arrival-rate set

$\{3.2, 1.6, 0.8, 0.4, 0.1, 0.05, 0.025, 0.0125, 0.00625, 0.003125\}$ . For each workload configuration, we further vary both the number of served adapters and the device configuration parameter  $A_{max}$  within the range 8 to 384. This process results in a large and heterogeneous training dataset that captures a wide range of workload conditions. Table 3 summarizes the prediction accuracy of the three evaluated ML model types (KNN, RF, and SVM), evaluated against the same real-system executions employed for the validation of the Digital Twin. Throughput prediction accuracy is quantified using SMAPE, while starvation detection performance is evaluated using macro-averaged F1 score across all scenarios.

Overall, the ML models achieve high predictive fidelity, particularly for starvation detection. Throughput prediction errors remain below 8%, slightly higher than those obtained using the Digital Twin, as expected given the additional abstraction introduced by the learning process. Fig. 8 additionally reports throughput predictions produced by the best-performing RF model, showing close agreement with real-system measurements. Prediction latency, also reported in Table 3, remains below 0.3 ms for all models except SVM, representing a substantial improvement over DT execution time.

Model	Estimator	Throughput		Starvation	
		SMAPE (%)	Time (ms)	F1 (macro)	Time (ms)
Llama	KNN	4.52	<b>0.21</b>	0.95	0.19
	RF	<b>4.39</b>	0.25	0.95	0.16
	SVM	6.84	1.70	<b>0.98</b>	<b>0.02</b>
Qwen	KNN	<b>5.28</b>	<b>0.15</b>	<b>0.99</b>	0.19
	RF	<b>5.28</b>	0.21	<b>0.99</b>	0.22
	SVM	7.46	2.24	0.93	<b>0.05</b>

Table 3: Final evaluation results of the proposed ML model across the three model types and both LLMs. It evaluates throughput estimation (with SMAPE) and starvation detection (with macro-F1), and reports the average prediction time in milliseconds.

**Refinement phase:** We further extend the ML learning phase with the refinement procedure described in Section 6. Table 4 reports results for the original RF model, the simplified shallow decision tree (*Small Tree*), and its Numba-optimized implementation (*Small Tree\*\**).

The refinement process yields substantial improvements in both inference efficiency and interpretability. The simplified models require at most 32 decision rules, compared to a minimum of 3.79e3 rules in the baseline RF. Inference latency is reduced by over 69× for the shallow tree and up to 2120× for the Numba-optimized implementation, achieving inference times below 100 ns per prediction in some occasions. These gains are obtained at the cost of reduced predictive accuracy. On average, throughput estimation exhibits a 6.74% increase in SMAPE, while starvation detection experiences a decrease of 0.025 in macro-F1 score. This trade-off remains acceptable in scenarios where inference speed and model interpretability are primary requirements.

Beyond performance improvements, the simplified models enable direct interpretability and extraction of actionable insights. Appendix C presents the learned decision trees for both starvation and throughput prediction. For instance, we can extract that starvation is unlikely when the aggregate incoming rate remains below 23.52 tokens/s, and that excessively large  $A_{max}$  values, above 144, can negatively impact overall system throughput.

#### 8.4. Caching decisions

We evaluate the proposed pipeline as a solution to the adapter caching problem, with the greedy algorithm acting as the final decision stage. We first analyze single-GPU scenarios to demonstrate throughput maximization and identification of the per-GPU optimal packing point ( $Max_{pack}$ ). We then extend the analysis to distributed settings with four GPUs, showing how consistently reaching  $Max_{pack}$  improves overall GPU efficiency, and comparing our approach against dLoRA. Finally, we evaluate an alternative configuration of the pipeline in which the optimization objective is shifted from resource efficiency to latency minimization.

The evaluation covers a diverse set of workload scenarios. Arrival rates are grouped into high-rate (2.4, 1.2, 0.6, 0.3, 0.15), low-rate (0.075, 0.0375, 0.01875, 0.009375, 0.0046875), and mixed-rate (0.6, 0.3, 0.15, 0.075, 0.0375) configurations, where adapter rates are randomly distributed from the considered configuration. Adapter sizes are also evaluated under varying settings, high-size (32), low-size (8), and mixed-size (8, 16, 32). For each workload configuration, the pipeline output is validated by executing the real LLM-adapter serving system, from which all reported figures and tables are obtained.

##### 8.4.1. Single-GPU system

To the best of our knowledge, there are no established baselines specifically addressing the adapter caching problem, i.e., identifying the optimal packing point  $Max_{pack}$

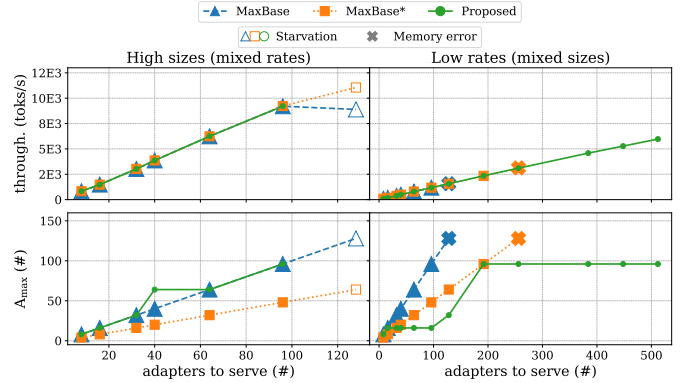


Figure 10: (Top) Achieved throughput and (Bottom) configured  $A_{max}$  on a single-GPU system for the allocations produced by the proposed pipeline and the two baselines under two settings. The left column shows results for Qwen and the right column for Llama. Each line extends until the corresponding strategy deems the allocation of the indicated number of adapters on the x-axis as infeasible, incurs in starvation or trigger memory errors.

jointly with an appropriate  $A_{max}$  configuration. We therefore introduce two simple yet reasonable reference strategies: *MaxBase* and *MaxBase\**. Both rely exclusively on the benchmarked maximum throughput of the backbone model, without accounting for adapter-specific dynamics or overheads, and differ only in how GPU parallelism is configured. In both cases, adapters are allocated to a GPU until the aggregate input rate reaches the backbone’s maximum throughput. *MaxBase* sets  $A_{max} = A$ , whereas *MaxBase\** constrains parallelism to  $A_{max} = A/2$ , where  $A$  is the number of adapters being served by the system.

Fig. 10 reports the throughput achieved by the real system and the configured  $A_{max}$  under the allocations generated by our pipeline and the two baselines, across two representative scenarios. In both scenarios, our approach identifies the optimal packing point  $Max_{pack}$ , achieving maximum feasible throughput while stopping before starvation or memory errors, which are treated as infeasible configurations. By contrast, the baselines—guided solely by backbone throughput—continue allocating beyond  $Max_{pack}$ , as they are unaware of adapter-induced overheads and serving dynamics. In the left scenario, both baselines incur starvation due to insufficient GPU memory to hold the requests KV cache. In the right scenario, they trigger memory errors by exceeding GPU capacity with overly large  $A_{max}$  values, first in *MaxBase* and subsequently in *MaxBase\**. These results highlight that our method adaptively adjusts  $A_{max}$  to workload conditions: while initially allowing high parallelism, it avoids excessive values to avoid memory errors, obtaining higher achievable throughput compared to both baselines.

##### 8.4.2. Distributed system

We now evaluate how accurate identification of  $Max_{pack}$  translates into improved GPU efficiency in distributed scenarios with four GPUs. We continue using the *MaxBase*

Model		No. rules	Throughput		No. rules	Starvation	
			SMAPE (%)	Time (ms)		F1 (macro)	Time (ms)
Llama	RF	7.13e6	<b>4.39</b>	0.25	4.44e4	<b>0.95</b>	0.16
	Small Tree	<b>32</b>	10.25	3.24e-3	<b>16</b>	0.92	3.25e-3
	Small Tree**	<b>32</b>	10.25	<b>1.13e-4</b>	<b>16</b>	0.92	<b>8.30e-5</b>
Qwen	RF	6.33e6	<b>5.28</b>	0.21	3.79e3	<b>0.99</b>	0.22
	Small Tree	<b>16</b>	12.89	2.52e-3	<b>15</b>	0.97	3.21e-3
	Small Tree**	<b>16</b>	12.89	<b>9.36e-5</b>	<b>15</b>	0.97	<b>10.5e-4</b>

Table 4: Evaluation results of the ML models obtained by progressively simplifying the best-performing RF model into a shallow, interpretable decision tree (Small Tree), and its Numba-optimized implementation (Small Tree\*\*).

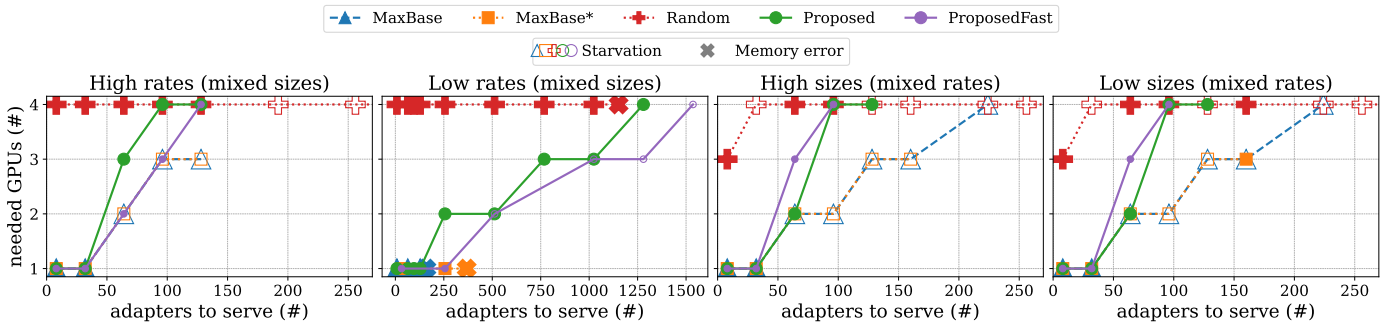


Figure 11: Number of GPUs required by each baseline and by the proposed pipeline on a 4-GPU system, across heterogeneous workloads with varying numbers of adapters, adapter sizes, and input rates. The two left plots correspond to Qwen and the two right plots to Llama. Each curve terminates when the corresponding method reaches an infeasible allocation, whereas *Random* is extended until starvation is clearly observed. Starvation or memory errors are extracted from running each method allocation in a real LLM-adapter serving system.

and *MaxBase\** baselines and additionally include a *Random* baseline, representing a trivial strategy that randomly assigns adapters to GPUs and samples  $A_{max}$  uniformly between 1 and the number of adapters allocated per GPU. Fig. 11 reports the number of GPUs that are used from the 4 available by each method to served adapters across heterogeneous workloads. The *Proposed* approach uses the best-performing ML model from Section 8.3, without the refinement phase, which is discussed later in this section.

As shown in the figure, the proposed pipeline dynamically adjusts the number of GPUs used for each workload. For example, in the leftmost scenario, when fewer than 50 adapters need to be served, all adapters are packed into a single GPU, while all four GPUs are only used once the number of adapters exceeds 80. The *MaxBase* and *MaxBase\** baselines exhibit a similar trend but propose allocations that lead to starvation or memory errors, as already observed in Section 8.4.1. In contrast, the *Random* baseline almost always utilizes all available GPUs, as expected. Overall, these results show that the proposed pipeline improves GPU efficiency by assigning the minimum number of GPUs required to serve a workload without incurring starvation or memory errors, effectively addressing the adapter caching problem. This is achieved by packing as many adapters as possible per utilized GPU while selecting an appropriate  $A_{max}$ , as discussed in Sec-

tion 8.4.1.

In addition, the proposed pipeline can sometimes serve more adapters without starvation within the four available GPUs than the baselines, as observed in the two middle scenarios (e.g., 1280 adapters in the second plot and 128 in the third). However, the opposite can also occur: in the rightmost scenario, *Random* reaches 160 adapters without starvation, while the proposed approach stops at 128. This behavior is expected given the stochastic nature of *Random*, which can occasionally find a feasible configuration by chance but is not reliable. Notably, while *Random*, *MaxBase*, and *MaxBase\** are highly unstable—frequently triggering memory errors or starvation—the proposed method consistently produces valid allocations.

Finally, Table 5 reports the execution time of the placement algorithms. The proposed approach is slower than the baselines for both single- and multi-GPU placements, taking approximately 2 seconds in the four-GPU case. This overhead is acceptable for the target use case of periodic reconfiguration under predictable workload patterns. Nevertheless, we further evaluate the faster variant, *ProposedFast*, which uses the *Small Tree\*\** model obtained in the refinement phase of Section 8.3. This variant reduces execution time to below 3 ms for four GPUs. However, this speedup comes at the cost of less stable predictions,

as illustrated by the second scenario in Fig. 11, due to the increased simplification of the learned model, which may be an acceptable tradeoff depending on the use case.

No.	Method	time(s)	
		Llama	Qwen
1	Proposed	1.54	0.43
	MaxBase	4.79e-4	5.38e-4
	MaxBase*	5.06e-4	5.54e-4
4	Proposed	2.16	2.18
	ProposedFast	2.17e-3	9.61e-4
	MaxBase	6.22e-4	5.28e-4
	MaxBase*	6.50e-4	5.40e-4
	Random	6.52e-4	6.37e-4
	dLoRAProactive	1.52e-1	2.34e-2

Table 5: Execution time of each baseline and of the two variants of the proposed pipeline, *Proposed* and *ProposedFast*, which respectively omit and include the refinement phase of the ML modeling stage.

#### 8.4.3. Comparison with dLoRA

To compare against a recent placement algorithm, we include an evaluation against dLoRA. Although dLoRA is primarily designed to minimize latency rather than to maximize GPU efficiency, it remains one of the few systems that proactively compute adapter placements for LLM-adapter serving. Given the limited prior work targeting utilization-oriented objectives, this comparison serves as a useful reference to highlight the practical differences between latency- and resource-driven optimization goals. We implement dLoRA variant with their original proactive placement code, which is originally periodically invoked to compute allocations for long-term workload patterns; other components of dLoRA are not included, as they are orthogonal to the adapter placement problem studied here.

Fig. 12 reports the required GPUs, throughput, and ITL for our pipeline (*Proposed*) and dLoRA across a set of heterogeneous scenarios, reflecting their contrasting objectives. Our approach aims to minimize the number of GPUs required to serve a workload while maintaining feasibility (i.e., avoiding starvation and memory errors), whereas dLoRA favors utilizing all available GPUs to reduce latency. As a result, our method consistently requires fewer GPUs, while dLoRA achieves lower latency at the cost of reduced GPU efficiency.

Besides, in the top scenario, dLoRA fails at large adapter counts due to a time-limit error, indicating that allocation computation does not scale to higher adapter number under our evaluation settings. This behavior is consistent with dLoRA’s original scope, which targets smaller adapter sets. In contrast, our approach continues

to scale and successfully serves significantly larger numbers of adapters. In the bottom scenario, dLoRA initially supports slightly more adapters and achieves higher peak throughput; however, as the workload increases further, it fails to detect starvation conditions, resulting in infeasible allocations. Our approach is more conservative in this case, stopping earlier and yielding lower peak throughput, but consistently avoiding starvation and memory errors.

Finally, Table 5 reports execution times for all placement algorithms. dLoRA is approximately one order of magnitude faster than our default pipeline. However, our refined variant, *ProposedFast*, achieves more than two orders of magnitude speedup over dLoRA, at the cost of less stable predictions, as discussed in the previous section.

#### 8.4.4. Latency oriented

To assess whether the proposed pipeline can be adapted to alternative objectives beyond GPU efficiency, we implement a proof-of-concept variant targeting latency minimization. This prototype, denoted *ProposedLat*, reuses the learned ML models but replaces the throughput-oriented greedy algorithm with a latency-oriented heuristic. Specifically, it assigns adapters sequentially to the GPU with the lowest aggregated arrival rate and configures  $A_{max}$  as the number of adapters served on each GPU. After all adapters are assigned, the resulting allocation is validated using the learned ML models; allocations predicted to trigger starvation or memory errors are deemed infeasible. Results for *ProposedLat* are included in Fig. 12 alongside the comparison with dLoRA.

Overall, *ProposedLat* tends to utilize all available GPUs, achieving latency comparable to dLoRA while consistently proposing allocations that do not incur in starvation or trigger memory errors. As expected, *ProposedLat* scales to fewer adapters than the default *Proposed* approach in the top scenario, primarily due to its trivial  $A_{max}$  configuration, which can over-reserve GPU memory. In the bottom scenario, *ProposedLat*, as discussed for default *Proposed* in previous section, remains more conservative than dLoRA, prioritizing feasible allocations over slight throughput improvements.

## 9. Discussion

Our evaluation shows that accurately identifying the single-GPU packing limit  $Max_{pack}$  is a key enabler for efficient adapter placement. As illustrated in Fig. 10, the proposed pipeline maximizes throughput while preventing infeasible configurations, stopping before starvation or memory errors and selecting an appropriate  $A_{max}$ . This highlights that, in LLM-adapter serving, adapter-induced overheads and the interaction between  $A_{max}$  and KV cache growth are essential for proposing feasible allocations. When extending the same decision logic to distributed settings (Fig. 11), the accurate identification of  $Max_{pack}$  translates directly into improved GPU efficiency.

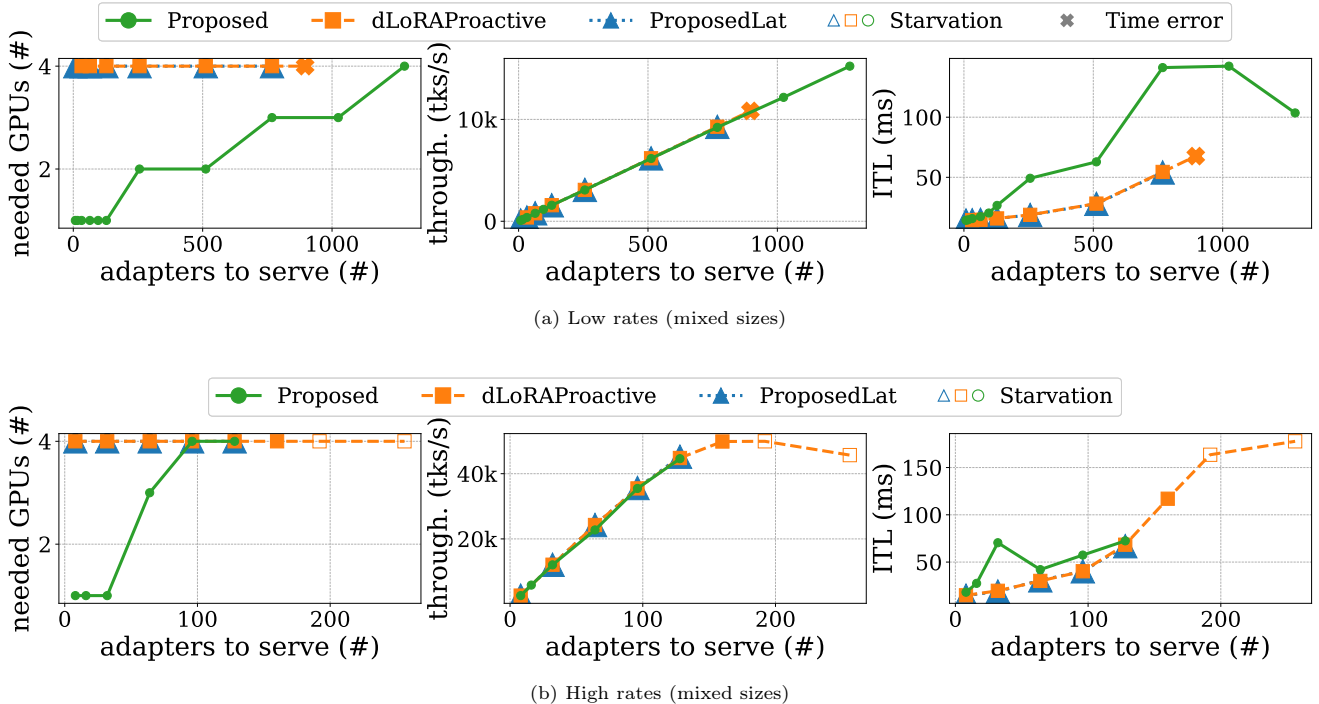


Figure 12: Number of GPUs required, throughput, and ITL achieved by each method on a 4-GPU system, across two heterogeneous workloads using Qwen. Each curve terminates when the corresponding method reaches an infeasible allocation. Starvation and memory errors are identified by executing the allocations on a real LLM-adapter serving system. The time-limit failure observed for dLoRA occurs when its placement algorithm does not complete within one hour for large numbers of adapters.

By packing adapters up to the feasibility boundary on each GPU, the pipeline dynamically determines the minimum number of GPUs required for a workload, reducing hardware usage whenever additional GPUs are not needed.

As shown in Table 5, the execution time required to compute allocations is compatible with the target use case of periodic reconfiguration under predictable workloads. Moreover, the optimized variant *ProposedFast*, obtained through refinement of the learned ML models, reduces execution time by orders of magnitude and is therefore better suited for scenarios where fast placement estimation is prioritized over prediction accuracy.

The comparison with dLoRA further emphasizes the impact of the optimization objective. dLoRA’s proactive mechanism is designed to minimize latency and therefore tends to use all available GPUs (Fig. 12). Our pipeline instead targets resource efficiency, using only the minimum number of GPUs needed to serve a given workload. Fig. 12 also includes a proof-of-concept latency-oriented variant of our method, *ProposedLat*, which achieves latency comparable to dLoRA while avoiding starvation and memory errors. This suggests that the proposed pipeline can be adapted to alternative optimization objectives, such as latency minimization, confirming its versatility beyond resource utilization.

Beyond its role in the proposed pipeline, the Digital Twin constitutes an additional contribution. To the best of our knowledge, it is the first Digital Twin specifically tailored to LLM-adapter serving. As shown in Table 1

and Figs. 8 and 9, it closely reproduces real-system performance—particularly throughput—across both predictable and unpredictable workloads, while operating significantly faster and at substantially lower computational cost (Table 2). This enables not only rapid synthetic dataset generation, but also broader applications such as scheduling optimization and server configuration.

Finally, Section 5.1 provided an in-depth characterization of LLM-adapter serving behavior, detailing the impact of the four principal overheads introduced by adapters. Beyond being the basis for the design and implementation of the proposed Digital Twin, this analysis offers independent value to the research community by exposing key system-level relationships, such as the connection between the adapter memory footprint overhead and the throughput plateau.

### 9.1. Limitations and future work

Although the Digital Twin supports dynamic input and output length distributions, the ML models are trained on simulations generated from a single dataset with a fixed request-length distribution. This limits generalization to workloads with substantially different sequence-length characteristics. Future work will extend dataset generation to cover diverse length distributions, enabling both the ML models and the placement algorithm to generalize to more heterogeneous serving conditions. In addition, our workload model assumes predictable Poisson arrivals parameterized by a per-adapter rate. While this

assumption is widely adopted in prior work and scheduling theory, real production traces may exhibit different predictable long-term arrival patterns, which should be incorporated in future evaluations.

## 10. Conclusions

We presented a data-driven pipeline to improve GPU efficiency in distributed LLM-adapter serving through workload-aware adapter placement. We evaluated the approach under heterogeneous workloads against multiple baselines, including a comparison with dLoRA’s proactive mechanism. The results show that the pipeline accurately identifies the feasible packing limit  $Max_{pack}$  and selects an appropriate  $A_{max}$  to maximize throughput and minimize the number of required GPUs to serve a given workload. The pipeline can be integrated into production systems to periodically update placements for predictable workload patterns, reducing the amount of needed hardware. The freed GPUs can be reassigned to other workloads to improve overall system efficiency or powered down to reduce energy consumption. Central to this approach is a high-fidelity Digital Twin for LLM-adapter serving, which closely reproduces real-system performance at low cost, enabling efficient ML training and supporting additional optimization tasks beyond this work.

## Acknowledgment

This work has been partially financed by the EU-HORIZON MSCA programme under grant agreement EU-HORIZON MSCA GA.101086248. Also, it has been partially financed by Generalitat de Catalunya (AGAUR) under grant agreement 2021-SGR-00478, by Severo Ochoa Center of Excellence CEX-2021-001148-S-20-3, and by the Spanish Ministry of Science (MICINN), the Research State Agency (AEI) and European Regional Development Funds (ERDF/FEDER) under grant agreement PID2021-126248OB-I00, MCIN/AEI/10.13039/501100011033/FEDER, UE.

The authors used OpenAI’s GPT model to assist with text rephrasing and stylistic refinement. All content was originally written and subsequently reviewed and validated by the authors.

## Appendix A. S-LoRA

We include a brief analysis using the S-LoRA framework [29] to show that the adapter caching problem is not specific to vLLM and also arises in other serving systems. Fig. A.13 reports the  $Max_{pack}$  point in S-LoRA across different arrival rates, for a fixed adapter size and a fixed request-length distribution, following the same methodology as the middle plot of Fig. 1 for vLLM. Notably, throughput degradation plateaus as the number of

adapters increases, whereas vLLM exhibits a more pronounced decline, highlighting the impact of S-LoRA’s design choices. Nevertheless, identifying  $Max_{pack}$  remains necessary to determine how many adapters can be allocated per GPU without triggering starvation, and the throughput level at which  $Max_{pack}$  occurs still varies across workloads, with additional variability expected when changing adapter sizes and request-length distributions.

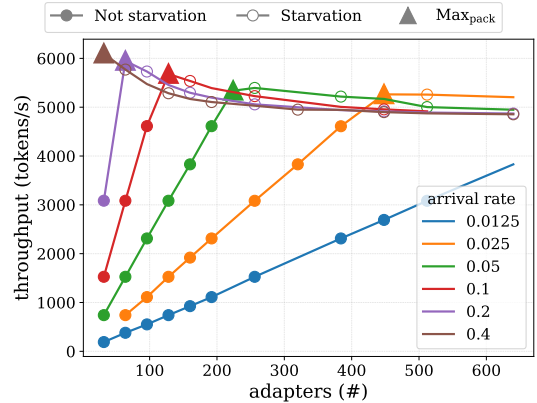


Figure A.13: Throughput obtained when running S-LoRA with varying adapter arrival rates on Llama-2-7B, using adapters of size 32 and requests with fixed lengths of 250 input tokens and 231 output tokens.

## Appendix B. ML hyperparameter search space

Hyperparameter optimization in the ML learning phase is performed using `HalvingGridSearchCV` with 5-fold cross-validation. Distinct search spaces are defined for the two tasks, throughput regression and starvation classification, using the corresponding scikit-learn model classes. The evaluated values for each hyperparameter are listed below.

**Throughput (Regression).** a) Random Forest (`RandomForestRegressor`): `n_estimators` {32,128,256}, `max_depth` {None,5,10,20}, `min_samples_split` {2,5,10,20}, `criterion` {squared\_error, absolute\_error, friedman\_mse, poisson}, `min_samples_leaf` {1,2,5,10,32,128}, `max_features` {auto,sqrt,log2}. b) SVM (SVR): `C` {0.1,1,10,100,1000,10000}, `kernel` {linear,poly,rbf,sigmoid}, `epsilon` {0.1,0.5,1,5}, `degree` {2,3,4,5}, `gamma` {scale,auto,0.01,0.1,1,10}, `coef0` {0,0.1,0.5,1}. c) KNN (`KNeighborsRegressor`): `p` {1,2}, with fixed `n_neighbors=1`, `leaf_size=8`, `weights=uniform`, `algorithm=kd_tree`.

**Starvation (Classification).** a) Random Forest (`RandomForestClassifier`): `n_estimators` {32,128,256}, `max_depth` {None,5,10,20}, `min_samples_split` {2,5,10,20}, `criterion` {gini,entropy,log\_loss}, `min_samples_leaf` {1,2,5,10,32,128}, `max_features` {None,sqrt,log2}. b) SVM (SVC): `C` {0.1,1,10,100,1000,10000}, `kernel`

{linear,poly,rbf,sigmoid}, degree {2,3,4,5}, gamma {scale,auto,0.01,0.1,1,10}, coef0 {0,0.1,0.5,1}. c) KNN (KNeighborsClassifier): p {1,2}, with fixed n\_neighbors=1, leaf\_size=8, weights=uniform, algorithm=kd\_tree.

## Appendix C. Derived lightweight tree estimators

Fig. C.14 depicts two of the shallow trees resulting from the refinement phase described in Section 6.

## References

- [1] Agrawal, A., Kedia, N., Mohan, J., Panwar, A., Kwatra, N., Gulavani, B.S., Ramjee, R., Tumanov, A., 2024a. Vidur: A large-scale simulation framework for llm inference. *Proceedings of Machine Learning and Systems* 6, 351–366.
- [2] Agrawal, A., Kedia, N., Panwar, A., Mohan, J., Kwatra, N., Gulavani, B., Tumanov, A., Ramjee, R., 2024b. Taming throughput-latency tradeoff in llm inference with sarathi-serve, in: *18th USENIX Symposium on Operating Systems Design and Implementation (OSDI 24)*, pp. 117–134.
- [3] anon8231489123, 2023. Clean sharegpt dataset. URL: [https://huggingface.co/datasets/anon8231489123/ShareGPT\\_Vicuna\\_unfiltered](https://huggingface.co/datasets/anon8231489123/ShareGPT_Vicuna_unfiltered).
- [4] Brown, T., Mann, B., Ryder, N., Subbiah, M., Kaplan, J.D., Dhariwal, P., Neelakantan, A., Shyam, P., Sastry, G., Askell, A., et al., 2020. Language models are few-shot learners. *Advances in neural information processing systems* 33, 1877–1901.
- [5] Brüel-Gabrielsson, R., Zhu, J., Bhardwaj, O., Choshen, L., Greenewald, K., Yurochkin, M., Solomon, J., 2024. Compress then serve: Serving thousands of lora adapters with little overhead. *arXiv preprint arXiv:2407.00066*.
- [6] Chen, L., Ye, Z., Wu, Y., Zhuo, D., Ceze, L., Krishnamurthy, A., 2024. Punica: Multi-tenant lora serving. *Proceedings of Machine Learning and Systems* 6, 1–13.
- [7] Cho, J., Kim, M., Choi, H., Heo, G., Park, J., 2024. Llm-servingsim: A hw/sw co-simulation infrastructure for llm inference serving at scale, in: *2024 IEEE International Symposium on Workload Characterization (IISWC)*, IEEE. pp. 15–29.
- [8] Garey, M.R., Johnson, D.S., 1979. *Computers and Intractability: A Guide to the Theory of NP-Completeness*. W. H. Freeman and Company, San Francisco.
- [9] Grattafiori, A., et al., 2024. The llama 3 herd of models. URL: <https://arxiv.org/abs/2407.21783>, arXiv:2407.21783.
- [10] Guo, D., Rush, A., Kim, Y., 2021. Parameter-efficient transfer learning with diff pruning, in: *Proceedings of the 59th annual meeting of the association for computational linguistics and the 11th international joint conference on natural language processing (volume 1: Long papers)*, pp. 4884–4896.
- [11] Houlsby, N., Giurgiu, A., Jastrzebski, S., Morrone, B., De Laroussilhe, Q., Gesmundo, A., Attariyan, M., Gelly, S., 2019. Parameter-efficient transfer learning for nlp, in: *International conference on machine learning*, PMLR. pp. 2790–2799.
- [12] Hu, E.J., Shen, Y., Wallis, P., Allen-Zhu, Z., Li, Y., Wang, S., Wang, L., Chen, W., et al., 2022. Lora: Low-rank adaptation of large language models. *ICLR* 1, 3.
- [13] Iliakopoulou, N., Stojkovic, J., Alverti, C., Xu, T., Franke, H., Torrellas, J., 2025. Chameleon: Adaptive Caching and Scheduling for Many-Adapter LLM Inference Environments. *Association for Computing Machinery, New York, NY, USA*. p. 217–231. URL: <https://doi.org/10.1145/3725843.3756083>.
- [14] Johnson, D.S., 1974. Fast algorithms for bin packing. *Journal of Computer and System Sciences* 8, 272–314. URL: <https://www.sciencedirect.com/science/article/pii/S0022000074800267>, doi:[https://doi.org/10.1016/S0022-0000\(74\)80026-7](https://doi.org/10.1016/S0022-0000(74)80026-7).
- [15] Kwon, W., Li, Z., Zhuang, S., Sheng, Y., Zheng, L., Yu, C.H., Gonzalez, J., Zhang, H., Stoica, I., 2023. Efficient memory management for large language model serving with pagedattention, in: *Proceedings of the 29th Symposium on Operating Systems Principles*, pp. 611–626.
- [16] Lam, S.K., Pitrou, A., Seibert, S., 2015. Numba: A llvm-based python jit compiler, in: *Proceedings of the Second Workshop on the LLVM Compiler Infrastructure in HPC*, pp. 1–6.
- [17] Li, S., Lu, H., Wu, T., Yu, M., Weng, Q., Chen, X., Shan, Y., Yuan, B., Wang, W., 2024. Caraserve: Cpu-assisted and rank-aware lora serving for generative llm inference. *arXiv preprint arXiv:2401.11240*.
- [18] Li, X.L., Liang, P., 2021. Prefix-tuning: Optimizing continuous prompts for generation. *Proceedings of the 59th Annual Meeting of the Association for Computational Linguistics and the 11th International Joint Conference on Natural Language Processing (Volume 1: Long Papers)*, 4582–4597 URL: <https://api.semanticscholar.org/CorpusID:230433941>.

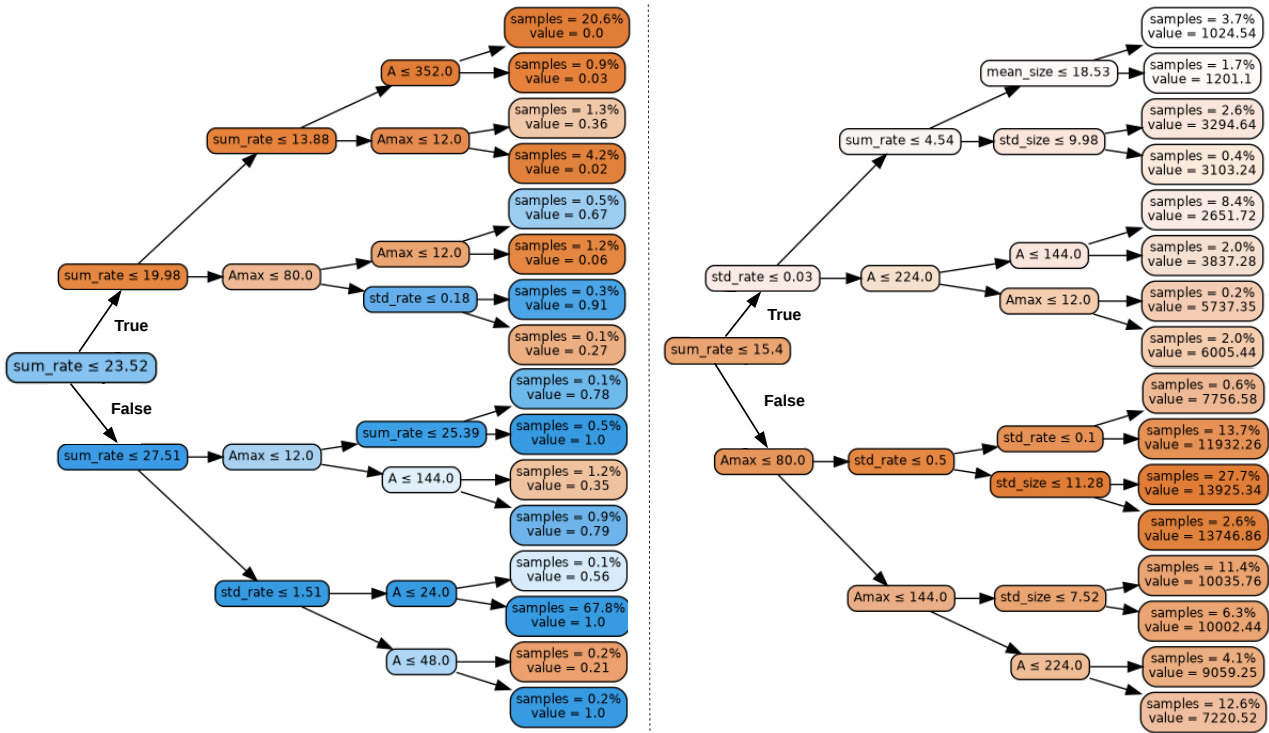


Figure C.14: Shallow decision trees derived from the best performing RF model to improve inference performance and enhance model interpretability. (Left) To estimate starvation for Llama-3.1-8B-Instruct. Final value represents the probability of starvation arising. (Right) To estimate throughput for Qwen2.5-7B-Instruct. Final value represents the expected throughput in toks/s.

[19] Liu, H., Tam, D., Muqeeth, M., Mohta, J., Huang, T., Bansal, M., Raffel, C.A., 2022. Few-shot parameter-efficient fine-tuning is better and cheaper than in-context learning. *Advances in Neural Information Processing Systems* 35, 1950–1965.

[20] López, F.A., Oliveras, J., Wang, C., Gutierrez-Torre, A., Tardieu, O., Youssef, A., Torres, J., Berral, J.L., 2025. A data-driven ml approach for maximizing performance in llm-adapter serving, in: *9th Machine Learning for Systems (ML for Systems) Workshop, NeurIPS 2025. Poster session, San Diego, CA*.

[21] Microsoft, 2022–2025. DeepSpeed-MII. GitHub repository. URL: <https://github.com/deepspeedai/DeepSpeed-MII>.

[22] NVIDIA, 2023–2025. TensorRT-LLM. GitHub repository. URL: <https://github.com/NVIDIA/TensorRT-LLM>.

[23] Pedregosa, F., Varoquaux, G., Gramfort, A., Michel, V., Thirion, B., Grisel, O., Blondel, M., Prettenhofer, P., Weiss, R., Dubourg, V., Vanderplas, J., Passos, A., Cournapeau, D., Brucher, M., Perrot, M., Duchesnay, E., 2011. Scikit-learn: Machine learning in Python. *Journal of Machine Learning Research* 12, 2825–2830.

[24] Qin, G., Eisner, J., 2021. Learning how to ask: Querying lms with mixtures of soft prompts, in: *Proceedings of the 2021 Conference of the North American Chapter of the Association for Computational Linguistics: Human Language Technologies*, pp. 5203–5212.

[25] Recasens, P.G., Agullo, F., Zhu, Y., Wang, C., Lee, E.K., Tardieu, O., Torres, J., Berral, J.L., 2025. Mind the memory gap: Unveiling gpu bottlenecks in large-batch llm inference, in: *2025 IEEE 18th International Conference on Cloud Computing (CLOUD)*, IEEE. pp. 277–287.

[26] Recasens, P.G., Zhu, Y., Wang, C., Lee, E.K., Tardieu, O., Youssef, A., Torres, J., Berral, J.L., 2024. Towards pareto optimal throughput in small language model serving, in: *Proceedings of the 4th Workshop on Machine Learning and Systems*, pp. 144–152.

[27] Shen, H., Chen, L., Jin, Y., Zhao, L., Kong, B., Philipose, M., Krishnamurthy, A., Sundaram, R., 2019. Nexus: a gpu cluster engine for accelerating dnn-based video analysis, in: *Proceedings of the 27th ACM Symposium on Operating Systems Principles*, Association for Computing Machinery, New York, NY, USA. p. 322–337. doi:10.1145/3341301.3359658.

- [28] Shen, Z., He, Y., Wang, Z., Zhang, Y., Sun, G., Ye, W., Li, A., 2025. EdgeLoRA: An Efficient Multi-Tenant LLM Serving System on Edge Devices. Association for Computing Machinery, New York, NY, USA. p. 138–153. URL: <https://doi.org/10.1145/3711875.3729141>.
- [29] Sheng, Y., Cao, S., Li, D., Hooper, C., Lee, N., Yang, S., Chou, C., Zhu, B., Zheng, L., Keutzer, K., et al., 2024. Slora: Scalable serving of thousands of lora adapters. Proceedings of Machine Learning and Systems 6, 296–311.
- [30] Sung, Y.L., Cho, J., Bansal, M., 2022. Lst: Ladder side-tuning for parameter and memory efficient transfer learning. Advances in Neural Information Processing Systems 35, 12991–13005.
- [31] Touvron, H., et al., 2023. Llama 2: Open foundation and fine-tuned chat models. URL: <https://arxiv.org/abs/2307.09288>, arXiv:2307.09288.
- [32] Wang, L., Chen, S., Jiang, L., Pan, S., Cai, R., Yang, S., Yang, F., 2025. Parameter-efficient fine-tuning in large language models: a survey of methodologies. Artificial Intelligence Review 58, 227. URL: <https://doi.org/10.1007/s10462-025-11236-4>, doi:10.1007/s10462-025-11236-4.
- [33] Wengwengwhale, 2024. Finance lora adapter for llama-3.1-8b instruct. URL: [https://huggingface.co/Wengwengwhale/llama\\_3.1\\_8B\\_Instruct\\_Finance\\_lora\\_adapter](https://huggingface.co/Wengwengwhale/llama_3.1_8B_Instruct_Finance_lora_adapter).
- [34] Wu, B., Zhu, R., Zhang, Z., Sun, P., Liu, X., Jin, X., 2024. dlora: Dynamically orchestrating requests and adapters for lora llm serving, in: 18th USENIX Symposium on Operating Systems Design and Implementation (OSDI 24), pp. 911–927.
- [35] Yang, A., et al., 2025. Qwen2.5 technical report. URL: <https://arxiv.org/abs/2412.15115>, arXiv:2412.15115.
- [36] yard1, 2024. Sql lora for llama-2-7b. URL: <https://huggingface.co/yard1/llama-2-7b-sql-lora-test>.
- [37] Yu, G.I., Jeong, J.S., Kim, G.W., Kim, S., Chun, B.G., 2022. Orca: A distributed serving system for transformer-based generative models, in: 16th USENIX Symposium on Operating Systems Design and Implementation (OSDI 22), pp. 521–538.
- [38] Zhang, H., Tang, Y., Khandelwal, A., Stoica, I., 2023. Shepherd: Serving dnns in the wild, in: 20th USENIX Symposium on Networked Systems Design and Implementation (NSDI 23), pp. 787–808.
- [39] zjudai, 2025. Medical lora for qwen2.5-7b-instruct. URL: <https://huggingface.co/zjudai/flowertune-medical-lora-qwen2.5-7b-instruct>.